This is a preprint, the final version is subject to change, of the American Mineralogist (MSA)
Cite as Authors (Year) Title. American Mineralogist, in press.
(DOI will not work until issue is live.) DOI: http://dx.doi.org/10.2138/am.2013.4260

Magnesite formation from MgO and CO_2 at the pressures and temperatures of Earth's mantle

Henry P. Scott[1], Vincent M. Doczy[1], Mark R. Frank[2], Maggie Hasan[2], Jung-Fu Lin[3], and Jing Yang[3]

[1]Department of Physics and Astronomy, IU South Bend, South Bend, IN 46634

[2]Department of Geology and Environmental Geosciences, Northern Illinois University, DeKalb, IL 60115

[3]Department of Geological Sciences, Jackson School of Geosciences, The University of Texas at Austin, Austin, TX 78712

Abstract

Magnesite formation from mixed oxides (MgO and CO_2) was observed in situ using synchrotron X-ray diffraction, coupled with laser-heated diamond anvil cells (DACs), at pressures and temperatures of Earth's mantle. Despite the existence of multiple high-pressure CO_2 polymorphs, the magnesite-forming reaction was observed to proceed at pressures ranging from 5 to 40 GPa and temperatures between 1,400 and 1,800 K. No other pressure-quenchable materials were observed to form via the $MgO + CO_2 = MgCO_3$ reaction. A large body of previous work has documented the stability of magnesite at elevated pressures and temperatures but, to the best of our knowledge, this is the first study to systematically demonstrate the formation of magnesite, rather than just the lack of a breakdown reaction, at

mantle pressures. Accordingly, this work further strengthens the notion that magnesite may indeed be the primary host phase for oxidized carbon in the deep Earth.

Keywords: Deep-carbon; magnesite; carbon dioxide; polymorphism

Introduction

The geological significance of carbon is clear due to its key roles in magmatic, metamorphic, eruptive and ore-formation processes (Ganino and Arndt 2009; Heijlen et al. 2008; Roberge et al. 2009; Tappert et al. 2009). Furthermore, the transport, cycling and storage of deep-Earth carbon are areas of intense, long-standing interest in which the interplay between atmospheric, crustal and mantle reservoirs is well appreciated (Hayes and Waldbauer 2006; Hirschmann and Dasgupta 2009; Ridgwell and Zeebe 2005; Sleep and Zahnle 2001). Due to its large volume (and therefore potentially large total carbon content), convective nature and direct connection to Earth's surface via subduction and volcanic exchanges, the mantle is particularly important for understanding carbon on a planetary scale. The relative abundance of oxidized carbon versus reduced carbon is difficult to quantify and is likely to vary with depth (e.g.Dasgupta and Hirschmann 2010), and there is abundant evidence regarding its complex mantle speciation, as indicated by the occurrence of carbonates in mantle-derived xenoliths (Berg 1986; Hervig and Smith 1981; McGetchin and Besancon 1973), kimberlitic diamonds, carbonatite magmas (Bell 1989) and prolific volcanic outgassing of CO_2 (Oppenheimer and Kyle 2008; Werner and Brantley 2003) and, occasionally, CH_4 (Fiebig et al. 2004).

There have been many petrologic studies in the CaO-MgO-SiO_2-CO_2-H_2O system (or a subset or slight expansion thereof) (Berg 1986; Brey et al. 1983; Brey and Green 1977; Katsura and Ito 1990; Koziol and Newton 1998; Kushiro 1975; Martinez et al. 1998; Newton and Sharp 1975; Olafsson and Eggler 1983; Wyllie 1977). The majority of these studies have been carried out in large-volume presses at pressures and temperatures (P-T) representative of the lower crust and upper mantle, where much of our current knowledge about the carbon-containing system lies.

A key conclusion from these early studies is the remarkable stability of carbonate minerals prior to decarbonation reactions at high temperatures. Although carbonate inclusions in xenoliths are fairly rare, likely due to decarbonation during exhumation (Canil 1990), numerous subsequent experimental studies have documented the striking stability of magnesite ($MgCO_3$) to very high P-T (Berg 1986; Biellmann et al. 1993; Canil 1990; Fiquet et al. 2002; Fiquet and Reynard 1999; Isshiki et al. 2004; Katsura and Ito 1990; Katsura et al. 1991; Litasov et al. 2008; Martinez et al. 1998; Ross 1997; Santillan et al. 2005). The high temperatures (3,000 K at 85 GPa (Isshiki et al. 2004)) achieved via laser-heated DACs strongly support the stability of magnesite to extreme P-T. Accordingly, carbonate is generally considered to be the dominant oxidized carbon species throughout much of the mantle, with magnesite, specifically, as the most abundant carbonate.

The predominance of magnesite at deep lower-mantle conditions, however, is less clear, as a structural transition to magnesite II at pressures greater than ~115 GPa has been observed (Isshiki et al. 2004; Panero and Kabbes 2008; Skorodumova et al. 2005). Additionally,

Boulard et al. (2011) demonstrated the formation of a $(CO_4)^{4-}$- structured phase in iron-containing magnesite ($(Mg,Fe)CO_3$) at pressures greater than 60 GPa, which is similar to a computationally predicted phase (Oganov et al. 2008), yet this new phase is expected to coexist with magnesite and diamond to great depths, especially if transported within a relatively cold subducting slab (Boulard et al. 2011). And, although pure magnesite has not been observed to dissociate into separate oxides such as MgO and CO_2 at the P-T of Earth's mantle, decarbonation reactions between magnesite and SiO_2, forming an assemblage of $MgSiO_3$-perovskite and CO_2, have been documented at lower-mantle P-T (Seto et al. 2008; Takafuji et al. 2006).

Furthermore, whereas some of the earlier large-volume press studies observed the formation of magnesite from CO_2 (typically introduced as $Ag_2C_2O_4$, silver oxalate), subsequent diamond anvil studies on the high-pressure (>~10 GPa) stability and high-temperature decarbonation of magnesite have generally relied on magnesite as a starting material as opposed to observing its formation from oxides. An exception to this is the work of Boulard et al (2011) who reacted both pure and iron-bearing MgO with CO_2 at pressures greater than 80 GPa in their work demonstrating the formation of a high-pressure carbon-bearing phase based on CO_4^{4-} units.

Notably, the phase diagram of CO_2 is complicated, and the high-pressure polymorphs are relatively dense and incompressible compared to "dry ice" (CO_2-I), which forms from the low-temperature deposition of gaseous CO_2 at ambient pressure or by the compression of liquid CO_2 to roughly 0.5 GPa at ambient temperature. Figure 1 shows an approximated

phase diagram for CO_2 as it is currently known for the P-T relevant to this study, following the recent experimental results and compilation of earlier work as summarized by Litasov et al. (2011); the figure is supported by data and interpretations from Tschauner et al. (2001), Santoro et al. (2004), Giordano et al. (2006), Giordano and Datchi (2007), Iota et al. (2007) and Datchi et al. (2009). It is important to note, however, that kinetic effects can be quite significant, and these are not necessarily equilibrium boundaries; Figure 1 is intended simply to summarize the CO_2 phases that one may expect in a study such as this, and some boundary locations, such as for the breakdown reaction from CO_2 to C + O_2, have been placed in different locations by previous workers. The reader is encouraged to refer to Litasov et al. (2011) or Sengupta et al. (2011) for a more thorough illustration of where these boundaries have been placed by different workers, or to Yoo et al. (2011a; 2011b) for extensions to even higher pressure conditions.

It is conceivable that such high-pressure CO_2 polymorphism could hinder the formation of magnesite even at moderate pressures. The motivation of the present study was to investigate magnesite formation in situ from CO_2 and MgO well within its range of expected stability. It is important to recognize a key caveat regarding these experiments, however, which is that they were all performed under CO_2-saturated conditions, and it is certainly not realistic to portray the mantle as having an activity of CO_2 close to unity ($a_{CO2} = 1$). That said, direct observations of the forward reaction, rather than the lack of a breakdown reaction, would strengthen the case for magnesite as a primary storage mineral for oxidized carbon in much of Earth's mantle.

Experimental

Symmetric-type diamond anvil cells (DACs) were used to contain and compress samples for all experiments, and infrared lasers were used for heating. The DACs utilized type I anvils with either 350 or 500 μm-diameter culets, depending on the desired experimental pressure, and 250-μm thick stainless steel (Type 301) was used as a gasket material. The gaskets were pre-indented to a thickness of between 60 and 80 μm, and sample chambers were drilled with diameters between 100 and 200 μm. For starting material, high-purity (>99.9%) Pt-black was added to pure MgO at the 3 wt% level to absorb infrared laser radiation, and this mixture was finely ground and pressed between two opposing anvils to form platelets approximately 20 μm thick.

A few grains of pure MgO were placed into the bottom of the sample chamber to hold the platelet above the anvil surface in order to avoid direct thermal contact with the anvil during laser heating. A piece of an MgO-Pt platelet, smaller than the diameter of the sample chamber, was then placed on the pure MgO grains in the center of the sample chamber. One or two grains of ruby of tens of microns in diameter were placed directly on the upper culet so that ruby fluorescence could be used to determine pressure during compression (Mao et al. 1978). The pressures reported in this paper, however, were determined by using X-ray diffraction and the equation of state (EoS) for MgO (Jacobsen et al. 2008); a 5% relative uncertainty in pressure was estimated for these measurements. Figure 2 shows a schematic illustration of the sample geometry and a photograph of an actual sample.

After loading and positioning the solid materials in the sample chamber, the entire cell was surrounded by liquid CO_2 using either the gas-loading system at the Carnegie Institution of Washington's Geophysical Laboratory in Washington D.C. or the gas-loading system at the GeoSoilEnviro Consortium for Advanced Radiation Sources (GSECARS) at Argonne National Laboratory. This was accomplished at room temperature by placing a slightly open DAC into a vessel that was subsequently pressurized to ~0.06 GPa (~8,000 p.s.i.) with pure CO_2. The DACs were then closed by remotely turning their screws to trap the CO_2. Raman spectroscopy was used subsequently to confirm the presence of CO_2 before further compression and heating.

X-ray diffraction measurements were conducted at the Advanced Photon Source (APS) of the Argonne National Laboratory at three different beamlines: 16-ID-B and 16-BM-D of the High-Pressure Collaborative Access Team (HPCAT) and 13-ID-D of GSECARS. The double-sided laser heating systems at 16-ID-B and 13-ID-D were used to overcome potential kinetic barriers for the formation of equilibrium assemblages. The temperatures reported here are not intended to represent the location of equilibrium phase boundaries in P-T space and, in most cases, are simply the lowest temperature at which sustained and consistent heating could be pyrometrically measured.

Analyses of diffraction patterns, after they were converted to one-dimensional profiles using FIT2D (Hammersley et al. 1996), were conducted in two stages. First, peak positions and intensities for expected phases were approximated using previously published diffraction information: unit cell data (i.e., crystal system and lattice parameters), Miller indicies (hkl's)

and observed relative intensities. For phases with well-known ambient-pressure structures and equations of state (K_{0T} and dK/dP), such as Pt, MgO, CO_2-I and magnesite, the high-pressure lattice parameters, and therefore d-spacings for the expected hkl's, could be readily calculated. Because the equations of state for the high-pressure CO_2 polymorphs are less well-constrained, estimates were made to calculate the lattice parameters at the pressure being considered. Unambiguous individual diffraction peaks attributed to each phase were then fit by Gaussian profiles to determine their d-spacings, and linear least-squares regression, coupled with their associated hkl's, was utilized to estimate the lattice parameters for each phase.

Subsequently, these estimated lattice parameters were used as starting values for whole-profile fitting with GSAS (Larson and Von Dreele 2000) utilizing the EXPGUI interface (Toby 2001). Due to the presence of multiple phases (up to five in some patterns) and some overlapping peaks, Rietveld structure refinement was found to be not feasible, but Le Bail whole-profile fitting was used to refine the lattice parameters for all phases satisfactorily.

Results and Discussion

Overview of Experiments Performed

Six laser-heating experiments were conducted at pre-heating pressures of 4.8(2), 10.9(5), 14.4(7), 22.3(11), 30.3(15) and 41.7(20) GPa, with a measured pressure drop of less than 10% after heating for most experiments. Although multiple diffraction patterns were typically collected before, during and after heating, these results will be discussed and presented as pre

and post heating diffraction pairs and grouped based on the CO_2 polymorphs observed prior to heating.

CO_2 Initially as CO_2-I

The experiments conducted at 4.8 and 10.9 GPa are relatively straightforward because they are in the CO_2-I stability field at room temperature, in which CO_2 crystalizes in the cubic system (space group Pa-3 (Downs and Somayazulu 1998)) with a well-constrained EoS (Giordano et al. 2010; Liu 1984; Olinger 1982). All pre-heating diffraction peaks at both pressures can be readily indexed as CO_2-I, MgO or Pt.

Measurable heating for the experiment at 4.8 GPa started at 1,300 K, but a temperature measurement could only be made from one side of the DAC, and this heating was sustained for forty minutes. Slightly higher laser power was used for the experiment at 10.9 GPa to facilitate pyrometric measurements from both sides of the DAC, and temperatures between 1,550 and 1,650 K were recorded and sustained for forty-five minutes. In both experiments new diffraction peaks were observed immediately upon heating, and the extended heating was conducted to see if it had a noticeable effect, but it appears to have been unnecessary.

The formation of magnesite after heating at 4.8 GPa (and a subsequent pressure drop to 4.7 GPa) can be unambiguously confirmed based on the new diffraction peaks observed, and there is no evidence for the formation of any other phases. The experiment at 10.9 GPa (10.3 GPa after heating) produced largely similar results in terms of clear magnesite formation, but only the strongest peak from CO_2-I remained readily apparent, and several new, but low-

intensity, peaks were present. Based on the pressure and heating history, either orthorhombic CO_2-III (space group Cmca (Aoki et al. 1994)) or rhombohedral CO_2-IV (space group *R*-3*c* (Datchi et al. 2009)) would be plausible candidate phases (e.g., Datchi et al. 2009; Park et al. 2003), but CO_2-IV is a much better match with the observed data. Table 1 presents a summary of unit-cell data for all phases observed in these experiments.

Decompression data were also collected for CO_2-I from the cell that was heated at 10.9 GPa, away from the heated region, to verify the EoS for CO_2-I. This was done due to an apparent discrepancy in the literature, with the earlier studies of Olinger (1982) and Liu (1984) producing similar EoS values (K_{0T} = 2.2 GPa, dK/dP = 6.4 and V_0 = 197.9 [$Å^3$ per unit cell] (our fit to the pressure-volume (P-V) data in Olinger (1982)) and K_{0T} = 2.93 GPa, dK/dP = 7.8 and V_0 = 208.6 [$Å^3$ per unit cell], respectively) compared to a more recent value of K_{0T} = 12 GPa reported by Yoo et al. (1999). Notably, Giordano et al. (2010) presented high-quality P-V-T EoS data with values quite similar to the earlier studies: K_{0T} = 3 GPa, dK/dP = 8.4 and V_0 = 200 [$Å^3$ per unit cell]. The results determined here are also similar: K_{0T} = 3.5 GPa, dK/dP = 9.1 GPa and V_0 = 197.9 [$Å^3$ per unit cell] (fixed based on the estimate of Olinger (1982)) and, as pointed out by Giordano et al. (2010), the variations in the studies with K_{0T} values near 3 GPa can be explained by the small differences in V_0 and covariance between K_{0T} and dK/dP. The much higher K_{0T} value reported by Yoo et al. (Yoo et al. 1999), however, is hard to interpret because it was not reported with values for V_0 or dK/dP.

CO_2 Initially as CO_2-III

As expected, carbon dioxide was present entirely as CO_2-III (space group Cmca (Aoki et al. 1994)) in the pre-heating patterns of experiments conducted at 14.4 and 22.0 GPa. Temperatures between 1,350 and 1,450 K were recorded during a heating duration of 20 minutes for the cell at 14.4 GPa, and the cell at 22.0 GPa heated stably at 1,550 K, which was sustained for 15 minutes. A summary of unit-cell data for all phases encountered both before and after heating can be seen in Table 2.

Post-heating, the cell initially at 14.4 GPa dropped to 13.1 GPa, whereas the cell initially at 22.0 GPa increased in pressure to 25.0 GPa – the only heating experiment observed to result in an increase in pressure after heating. As with the experiment at 10.9 GPa, temperature-quenched patterns from both of these experiments included CO_2-IV, rather than CO_2-III, but tetragonal CO_2-II (space group $P4_2/mnm$ (Yoo et al. 2002)) is present in the post-heat pattern at 25 GPa as well.

The formation of magnesite was clear and unambiguous in both experiments, but the experiment at 14.4 GPa produced a few unaccounted for peaks at 1.669, 1.587 and 1.423 Å. These peaks are low in intensity, but they are sharp and spotty, and clearly form distinct diffraction rings on the image plate. Notably, quenching from the liquid phase of CO_2 at this pressure would be consistent with the formation of orthorhombic CO_2-VII (space group *Cmca* (Giordano and Datchi 2007)), but with so much of the pattern obscured by stronger reflections from other phases, it is not possible to make a conclusive determination.

250 **CO_2 Initially as CO_2-IV**

251 Prior to heating, only one diffraction line is visually attributable to CO_2 for either of the
252 experiments conducted at 30.3 and 41.7 GPa, and in both cases it appears to be due to
253 overlapping (024) and (220) reflections from the CO_2-IV structure. Given that these are pre-
254 heating patterns one may expect the CO_2-III structure, but it should be noted that spatially
255 separated locations in both DACs, from the same loading, had already been heated at lower
256 pressures. Neither of the pre-heating patterns shows evidence for the presence of magnesite,
257 yet it is likely that heating elsewhere in the cells (approximately 50 to 100 μm away) warmed
258 the cells sufficiently to convert all of the CO_2 to the CO_2-IV structure.
259
260 During heating, however, more CO_2 diffraction lines became apparent from both cells, and
261 some of the CO_2 transformed to the tetragonal CO_2-V structure (space group *I*-42*d* (Datchi et
262 al. 2012)), whereas some remained as CO_2-IV. The cell at 30.3 GPa was heated for
263 approximately 60 minutes, with momentary peak temperature measurements of >2,700 K for
264 both sides, but sustainable measurements were in the range of 1,900 to 2,100 K. The post-
265 heating pressure was 30.1 GPa. For the cell at 41.7 GPa, sustained temperature measurements
266 were between 1,600 and 1,800 K with a similar duration of 60 minutes; upon temperature
267 quench, the pressure was 37.8 GPa. Notably, this was the only heating experiment for which
268 all of the CO_2 should have remained within the solid state, as can be seen in Figure 1.
269
270 As with the lower-pressure experiments, the heating experiments at 30.3 and 41.7 GPa both
271 produced clear and unambiguous diffraction patterns indicative of magnesite, and a summary
272 of all phases observed pre and post heating can be seen in Table 3. Figure 3 shows pre- and

post-heating patterns for the 41.7 GPa heating experiment. This experiment was chosen to display representative patterns because, as the highest-pressure experiment conducted in this study, it is arguably the most significant in terms of demonstrating the formation of magnesite at mantle pressures.

The upper panels in Figure 3 show the results of fitting from within EXPGUI / GSAS, and the residuals are shown at the bottom. The lower panels show the same patterns, but they have been converted to d-spacing, the backgrounds have been subtracted, and the dominant MgO peaks have been truncated to better show peaks from the other phases. Furthermore, the vertical sticks on the lower panel have been scaled so that the most intense peak for each phase matches the greatest intensity observed for that phase. The remaining relative scaled intensities, however, are from the previously determined structures of other workers, and they are intended to provide an additional indication of the overall appropriateness of the phase identifications.

Although the integrated relative intensities for magnesite peaks show good agreement with those of previous workers, this is somewhat fortuitous because the data from the actual image plate are spotty as shown in Figure 4, which would be expected for crystal growth during laser heating. Although the most intense reflection from (104) can be identified as an individual ring, other reflections such as (202) manifest primarily as a few discrete spots with only very faint rings visible, if at all.

Both of these cells were subsequently decompressed, and all peaks in the ambient-pressure diffraction patterns can be readily indexed as magnesite, MgO or Pt. No peaks ascribed to CO_2 at high pressures persist to ambient pressure, and there are no unexpected peaks.

Anisotropic Compression in Magnesite

Because all of the magnesite observed in these experiments crystallized under simultaneous high P-T conditions, with the surrounding CO_2 above or very near its melting point, we would expect the deviatoric stress on the crystals to be fairly low. This is superficially supported by their narrow diffraction lines at all pressures. Our measured lattice-parameter axial ratios (i.e. c/a), along with those from previous workers (Fiquet et al. 2002; Fiquet and Reynard 1999; Ross 1997), are plotted against pressure in Figure 5 to compare our results with previous compressional data collected in both hydrostatic and non-hydrostatic conditions.

Fiquet et al. (1999) used a variety of pressure-transmitting media to surround the magnesite; their data collected in Argon and methanol-ethanol water (MEW) are essentially indistinguishable from the single-crystal data collected in methanol-ethanol (ME) by Ross (1997) over the pressure range for which they overlap, which is limited to pressures below about 9 GPa. Notably, this pressure is approximately where both ME and MEW solidify and, accordingly, non-hydrostaticity is expected. Fiquet et al. (2002), conversely, did not use any pressure-transmitting medium and, instead, used laser heating to thoroughly anneal the sample at each pressure step. An exponential trend can readily fit both their high-pressure data and the truly hydrostatic data points of Ross (1997) and Fiquet et al. (1999). The non-hydrostatic data points from Fiquet et al. (1999), however, clearly deviate to lower c/a values, strongly

318 suggesting that deviatoric stress enhances the known anisotropic compression of magnesite.
319 Our data show good agreement with this trend, but our datum at 25 GPa is at a higher *c*/*a*
320 value than it would predict. Overall, however, it appears that the laser-annealing technique
321 employed by Fiquet et al. (2002) does indeed relieve the deviatoric stress as intended.
322
323 **Thermodynamics of Magnesite Formation**
324 To accurately model the thermodynamic stability of magnesite relative to CO_2 and MgO at
325 elevated P-T, one would need not only reference-state free energies, but also P-T-dependent
326 entropy and EoS data for all phases. Fiquet et al. (2002) created such a model using a
327 combination of theoretically calculated and experimentally measured values to predict the
328 equilibrium curve to pressures of 150 GPa and temperatures of 5,000 K. They noted the
329 importance of volumetric effects, particularly at high pressure, and they concluded that
330 temperatures well above the geotherm would be necessary for the decarbonation of magnesite.
331
332 As a simple demonstration of this volumetric importance using the data presented in this
333 study, Figure 6 shows the ΔV, in terms of molar volumes, of the reaction $CO_2 + MgO =$
334 $MgCO_3$ upon temperature quench. The negative ΔV for calculations based on observations of
335 quenched CO_2-I and CO_2-IV would indeed serve to drive the reaction toward magnesite
336 production. However, the positive ΔV for calculations based on observations of quenched
337 CO_2-V would serve to inhibit the reaction. This does not, of course, suggest that the reaction
338 should not proceed at high temperatures, but rather that an entropic term, or thermal
339 expansion, dominates in this case. That said, this is a significant observation because it does

suggest that relatively dense high-pressure polymorphs in CO_2, such as CO_2-V, could serve to disfavor the magnesite-forming reaction at low temperatures.

Concluding Remarks

As expected based on a large body of previous work demonstrating its remarkable stability at high P-T, magnesite readily forms from CO_2 and MgO at pressures between 5 and 40 GPa and temperatures from 1,400 to 1,800 K. Indeed, even at the highest pressure of this study, and with CO_2 in the relatively dense CO_2-IV structure, the reaction to form magnesite proceeded at temperatures below 1,800 K.

The true significance of magnesite for carbon storage in the lower mantle remains a complicated issue that will, of course, depend on a number of critical parameters such as total carbon budget, relative partitioning between carbonates and silicates (Panero and Kabbes 2008) and oxygen fugacity (Frost and McCammon 2008). Indeed, the redox state at which carbonate would be reduced to diamond has been determined, based on buffered multianvil experiments, to be well above the iron-wüstite buffer (Stagno et al. 2011). Furthermore, recent work demonstrates that fO_2 decreases with increasing depth, at least in the upper mantle and, accordingly, carbon is likely present in reduced phases and oxidation does not occur until there is upwelling (Stagno et al. 2013).

Additionally, observations of high-pressure polymorphism (Isshiki et al. 2004) and newly discovered carbon-bearing phases (Boulard et al. 2011; Oganov et al. 2008) obscure the significance of the ambient-pressure magnesite structure at the greatest mantle depths. That

said, the remarkable ease with which magnesite forms from MgO and CO_2, as shown in this study, further supports the notion that it is indeed one of the dominant storage phases for oxidized carbon in much of Earth's interior.

Acknowledgements

We gratefully acknowledge M. Somayazulu for gas loading at the Geophysical Lab; Y. Meng and D. Popov (HPCAT) and V. Prakapenka (GSECARS) for scientific and beamline support at APS; and E. Borkholder, E. Cotter and T. Kinney for experimental assistance. The majority of this work was performed at HPCAT (Sector 16), Advanced Photon Source (APS), Argonne National Laboratory. HPCAT is supported by CIW, CDAC, UNLV and LLNL through funding from DOE-NNSA, DOE-BES and NSF. APS is supported by DOE-BES, under Contract No. DE-AC02-06CH11357. Use of 16-IDB was supported by HiPSEC, UNLV, through NNSA Cooperative agreement DE-FC-06NA27684. A portion of this work was also performed at GeoSoilEnviroCARS (Sector 13), Advanced Photon Source (APS), Argonne National Laboratory. GeoSoilEnviroCARS is supported by the National Science Foundation - Earth Sciences (EAR-0217473), Department of Energy - Geosciences (DE-FG02-94ER14466) and the State of Illinois. This research was partially supported by COMPRES, the Consortium for Materials Properties Research in Earth Sciences under NSF Cooperative Agreement EAR 11-57758. H. Scott thanks the IUSB R&D committee for faculty research support and the SMART committee for supporting several undergraduate researchers who helped with this project. J.F. Lin acknowledges supports from NSF-EAR Geophysics, CDAC (Carnegie-DOE Alliance Center), and EFree (Energy Frontier Research in Extreme Environments).

References Cited

Aoki, K., Yamawaki, M., Sakashita, M., Gotoh, Y., and Takemura, K. (1994) Crystal Structure of the High-Pressure Phase of Solid CO_2. Science, 263, 356-358.

Bell, K. (1989) Carbonatites: Genesis and evolution, p. 618. Unwin Hyman, London.

Berg, G.W. (1986) Evidence for carbonate in the mantle. Geology, 324, 50-51.

Biellmann, C., Gillet, P., Guyot, F., Peyronneau, J., and Reynard, B. (1993) Experimental evidence for carbonate stability in the Earth's lower mantle. Earth and Planetary Science Letters, 118, 31-41.

Boulard, E., Gloter, A., Corgne, A., Antonangeli, D., Auzende, A.L., Perrillat, J.P., Guyot, F., and Fiquet, G. (2011) New host for carbon in the deep Earth. Proceedings of the National Academy of Sciences of the United States of America, 108, 5184-5187.

Brey, G., Brice, W.R., Ellis, D.J., Green, D.H., Harris, K.L., and Ryabchikov, I.D. (1983) Pyroxene-carbonate reactions in the upper mantle. Earth and Planetary Science Letters, 62, 63-74.

Brey, G., and Green, D.H. (1977) Systematic study of liquidus phase relations in olivine melilitite + H_2O + CO_2 at high pressures and petrogenesis of an olivine melilitite magma. Contributions to Mineralogy and Petrology, 61, 141-162.

Canil, D. (1990) Experimental study bearing on the absence of carbonate in mantle-derived zenoliths. Geology, 18, 1011-1013.

Dasgupta, R., and Hirschmann, M.M. (2010) The deep carbon cycle and melting in Earth's interior. Earth and Planetary Science Letters, 298, 1-13.

Datchi, F., Giordano, V.M., Munsch, P., and Saitta, A.M. (2009) Structure of Carbon Dioxide Phase IV: Breakdown of the Intermediate Bonding State Scenario. Physical Review Letters, 103, 10.1103/PhysRevLett.103.185701.

Datchi, F., Mallick, B., Salamat, A., and Ninet, S. (2012) Structure of Polymeric Carbon Dioxide CO_2-V. Physical Review Letters, 108, 10.1103/PhysRevLett.108.125701.

Downs, R.T., and Somayazulu, M.S. (1998) Carbon dioxide at 1.0 GPa. Acta Crystallographica Section C-Crystal Structure Communications, 54, 897-898.

Fiebig, J., Chiodini, G., Caliro, S., Rizzo, A., Spangenberg, J., and Hunziker, J.C. (2004) Chemical and isotopic equilibrium between CO_2 and CH_4 in fumarolic gas discharges: Generation of CH_4 in arc magmatic-hydrothermal systems. Geochimica et Cosmochimica Acta, 68, 2321-2334.

Fiquet, G., Guyot, F., Kunz, M., Matas, J., Andrault, D., and Hanfland, M. (2002) Structural refinements of magnesite at very high pressure. American Mineralogist, 87, 1261-1265.

Fiquet, G., and Reynard, B. (1999) High-pressure equation of state of magnesite: New data and a reappraisal. American Mineralogist, 84, 856-860.

Frost, D.J., and McCammon, C.A. (2008) The redox state of Earth's mantle. Annual Review of Earth and Planetary Sciences, 36, 389-420.

Ganino, C., and Arndt, N.T. (2009) Climate changes caused by degassing of sediments during the emplacement of large igneous provinces. Geology, 37, 323-326.

Giordano, V.M., and Datchi, F. (2007) Molecular carbon dioxide at high pressure and high temperature. Europhysics Letters, 77, 10.1209/0295-5075/77/46002.

Giordano, V.M., Datchi, F., and Dewaele, A. (2006) Melting curve and fluid equation of state of carbon dioxide at high pressure and high temperature. Journal of Chemical Physics, 125, 10.1063/1.2215609

Giordano, V.M., Datchi, F., Gorelli, F.A., and Bini, R. (2010) Equation of State and Anharmonicity of Carbon Dioxide Phase I Up to 12 GPa and 800 K. Journal of Chemical Physics, 133, 10.1063/1.3495951.

Hammersley, A.P., Svensson, S.O., Hanfland, M., Fitch, A.N., and Häusermann, D. (1996) Two-dimensional detector software: From real detector to idealised image or two-theta scan. High Pressure Research, 14, 235-248.

Hayes, J.M., and Waldbauer, J.R. (2006) The carbon cycle and associated redox processes through time. Phil. Trans. R. Soc. Lond., 361, 931-950.

Heijlen, W., Banks, D.A., Muchez, P., Stensgard, B.M., and Yardley, B.W.D. (2008) The Nature of Mineralizing Fluids of the Kipushi Zn-Cu Deposit, Katanga, Democratic Repubic of Congo: Quantitative Fluid Inclusion Analysis using Laser Ablation ICP-MS and Bulk Crush-Leach Methods. Economic Geology, 103, 1459-1482.

Hervig, R.L., and Smith, J.V. (1981) Dolomite-apatite incluion in chrome-diapside crystal, Bellsbank kimberliet, South Africa. American Mineralogist, 66, 346-349.

Hirschmann, M.M., and Dasgupta, R. (2009) The H/C ratios of Earth's near-surface and deep reservoirs, and consequences for deep Earth volatile cycles. Chemical Geology, 262, 4-16.

Iota, V., Yoo, C.S., Klepeis, J.H., Jenei, Z., Evans, W., and Cynn, H. (2007) Six-fold coordinated carbon dioxide VI. Nature Materials, 6, 34-38.

Isshiki, M., Irifune, T., Hirose, K., Ono, S., Ohishi, Y., Watanuki, T., Nishibori, E., Takata, M., and Sakata, M. (2004) Stability of magnesite and its high-pressure form in the lowermost mantle. Nature, 427, 60-63.

Jacobsen, S.D., Holl, C.M., Adams, K.A., Fischer, R.A., Martin, E.S., Bina, C.R., Lin, J.F., Prakapenka, V.B., Kubo, A., and Dera, P. (2008) Compression of single-crystal magnesium oxide to 118 GPa and a ruby pressure gauge for helium pressure media. American Mineralogist, 93, 1823 - 1828.

Katsura, T., and Ito, E. (1990) Melting and subsolidus phas relations in the $MgSiO_3$-$MgCO_3$ system at high-pressures: Implications to evolution of the Earth's atmosphere. Earth and Planetary Science Letters, 99, 110-117.

Katsura, T., Tsuchida, Y., Ito, E., Yagi, T., Utsumi, W., and Akimoto, S. (1991) Stability of magnesite under the lower mantle conditions. Proceedings of the Japan Academy, 67, 57-60.

Koziol, A.M., and Newton, R.C. (1998) Experimental determination of the reaction: Magnesite + enstatite = forsterite + CO_2 in the ranges 6-25 kbar and 700-1100 °C. American Mineralogist, 83, 213-219.

Kushiro, I. (1975) Carbonate-silicate reactions at high pressures and possible presence of dolomite and magnesite in the upper mantle. Earth and Planetary Science Letters, 28, 116-120.

Larson, A.C., and Von Dreele, R.B. (2000) General Structure Analysis System (GSAS), p. 86-748. Los Alamos National Laboratory Report LAUR.

Litasov, K.D., Fei, Y.W., Ohtani, E., Kuribayashi, T., and Funakoshi, K. (2008) Thermal equation of state of magnesite to 32 GPa and 2073 K. Physics of the Earth and Planetary Interiors, 168, 191-203.

Litasov, K.D., Goncharov, A.F., and Hemley, R.J. (2011) Crossover from melting to dissociation of CO_2 under pressure: Implications for the lower mantle. Earth and Planetary Science Letters, 10.1016/j.epsl.2011.07.006.

Liu, L. (1984) Compression of Solid CO_2 to half a megabar. Earth and Planetary Science Letters, 71, 104-110.

Mao, H.K., Bell, P.M., Shaner, J.W., and Steinberg, D.J. (1978) Specific volume measurements of Cu, Mo, Pd, and Ag and calibration of the ruby R_1 fluorescence pressure gauge from 0.06 to 1 Mbar. Journal of Applied Physics, 49, 3276-3283.

Martinez, I., Perez, E.M.C., Matas, J., Gillet, P., and Vidal, G. (1998) Experimental investigation of silicate-carbonate system at high pressure and high temperature. Journal of Geophysical Research, 103, 5143-5163.

McGetchin, T.R., and Besancon, J.R. (1973) Carbonate inclusions in mantle-derived pyropes. Earth and Planetary Science Letters, 18, 408-410.

Newton, R.C., and Sharp, W.E. (1975) Stability of forsterite + CO_2 and its bearing on the role of CO_2 in the mantle. Earth and Planetary Science Letters, 26, 239-244.

Oganov, A.R., Ono, S., Ma, Y.M., Glass, C.W., and Garcia, A. (2008) Novel high-pressure structures of $MgCO_3$, $CaCO_3$ and CO_2 and their role in Earth's lower mantle. Earth and Planetary Science Letters, 273, 38-47.

Olafsson, M., and Eggler, D.H. (1983) Phase Relations of Amphibole, Ambibole-Carbonate, and phlogopite-carbonate peridotite: petrologic constraints on the asthenosphere. Earth and Planetary Science Letters, 64, 305-315.

Olinger, B. (1982) The compression of solid CO_2 at 296 K to 10 GPa. Journal of Chemical Physics, 77, 6255-6258.

Oppenheimer, C., and Kyle, P.R. (2008) Probing the magma plumbing of Erebus volcano, Antarctica, by open-path FTIR spectroscopy of gas emissions. Journal of Volcanology and Geothermal Research, 177, 743-754.

Panero, W.R., and Kabbes, J.E. (2008) Mantle-wide sequestration of carbon in silicates and the structure of magnesite II. Geophysical Research Letters, 35, 10.1029/2008gl034442.

Park, J.H., Yoo, C.S., Iota, V., Cynn, H., Nicol, M.F., and Le Bihan, T. (2003) Crystal structure of bent carbon dioxide phase IV. Physical Review B, 68, 10.1103/PhysRevE.68.014107.

Ridgwell, A., and Zeebe, R.E. (2005) The role of the global carbonate cycle in the regulation and evolution of the Earth system. Earth and Planetary Science Letters, 234, 299-315.

Roberge, J., Delgado-Granados, H., and Wallace, P.J. (2009) Mafic magma recharge supplies high CO_2 and SO_2 gas fluxes from Popocatepetl volcano, Mexico. Geology, 37, 107-110.

Ross, N.L. (1997) The equation of state and high-pressure behavior of magnesite. American Mineralogist, 82, 682-688.

Santillan, J., Catalli, K., and Williams, Q. (2005) An infrared study of carbon-oxygen bonding in magnesite to 60 GPa. American Mineralogist, 90, 1669-1673.

Santoro, M., Lin, J.F., Mao, H.K., and Hemley, R.J. (2004) In situ high P-T Raman spectroscopy and laser heating of carbon dioxide. Journal of Chemical Physics, 121, 2780-2787.

Sengupta, A., Kim, M., Yoo, C.S., and Tse, J.S. (2011) Polymerization of carbon dioxide: A chemistry view of molecular-to-nonmolecular phase transitions. The Journal of Physical Chemistry C, 116, 2061-2067.

Seto, Y., Hamane, D., Nagai, T., and Fujino, K. (2008) Fate of carbonates within oceanic plates subducted to the lower mantle, and a possible mechanism of diamond formation. Physics and Chemistry of Minerals, 35, 223-229.

Skorodumova, N.V., Belonoshko, A.B., Huang, L., Ahuja, R., and Johansson, B. (2005) Stability of the $MgCO_3$ structures under lower mantle conditions. American Mineralogist, 90, 1008-1011.

Sleep, N.H., and Zahnle, K. (2001) Carbon dioxide cycling and implications for climate on ancient Earth. Journal of Geophysical Research, 106, 1373-1399.

Stagno, V., Ojwang, D.O., McCammon, C.A., and Frost, D.J. (2013) The oxidation state of the mantle and the extraction of carbon from Earth's interior. Nature, 493, 84-88.

Stagno, V., Tange, Y., Miyajima, N., McCammon, C.A., Irifune, T., and Frost, D.J. (2011) The stability of magnesite in the transition zone and the lower mantle as function of oxygen fugacity. Geophysical Research Letters, 38, L19309.

Takafuji, N., Fujino, K., Nagai, T., Seto, Y., and Hamane, D. (2006) Decarbonation reaction of magnesite in subducting slabs at the lower mantle. Physics and Chemistry of Minerals, 33, 651-654.

Tappert, R., Foden, J., Stachel, T., Muehlenbachs, K., Tappert, M., and Wills, K. (2009) Deep mantle diamonds from South Australia: A record of Pacific subduction at the Gondwanan margin. Geology, 37, 43-46.

Toby, A.P. (2001) EXPGUI, a graphical user interface for GSAS. J. Appl. Cryst., 34, 210-213.

Tschauner, O., Mao, H.K., and Hemley, R.J. (2001) New transformations of CO_2 at high pressures and temperatures. Physical Review Letters, 87, 10.1103/PhysRevLett.87.075701.

Werner, C., and Brantley, S. (2003) CO_2 emissions from the Yellowstone volcanic system. Geochemistry Geophysics Geosystems, 4, 10.1029/2002gc000473.

Wyllie, P.J. (1977) Mantle fluid compositions buffered by carbonates in peridotite-CO_2-H_2O. Journal of Geology, 85, 187 - 207.

Yoo, C.S., Cynn, H., Gygi, F., Galli, G., Iota, V., Nicol, M., Carlson, S., Hausermann, D., and Mailhiot, C. (1999) Crystal structure of carbon dioxide at high pressure: "Superhard" polymeric carbon dioxide. Physical Review Letters, 83, 5527-5530.

Yoo, C.S., Kohlmann, H., Cynn, H., Nicol, M.F., Iota, V., and LeBihan, T. (2002) Crystal structure of pseudo-six-fold carbon dioxide phase II at high pressures and temperatures. Physical Review B, 65, 10.1103/PhysRevB.65.104103.

Yoo, C.S., Sengupta, A., and Kim, M. (2011a) Carbon dioxide carbonates in the Earth's mantle: Implications to the deep carbon cycle. Angewandte Chemie International Edition, 50, 11219-11222.

-. (2011b) Phase diagram of carbon dioxide: update and challenges. High Pressure Research, 31, 68-74.

564

565 **Figure and Table Captions**

566

567 **Figure 1.** A simplified phase diagram of CO_2, after the summarizing figure of recent
568 work presented by Litasov et al. (2011). The superimposed data points are the P-T conditions
569 encountered during the laser-heating measurements of this study.

570

571 **Figure 2.** **(a)** Schematic for loaded sample chamber: Pt black was used to absorb infrared
572 laser radiation and the pure MgO grains were used as a substrate to thermally isolate the
573 MgO-Pt platelet from the anvils during heating. **(b)** A photograph of a loaded sample as
574 viewed from above. This particular loading had to spatially separate platelets, one that is
575 roughly square and the other roughly triangular; this readily allowed for two heating
576 experiments to be conducted at different pressures.

577

578 **Figure 3.** Diffraction patterns collected before and after leaser heating at 41.7 GPa; a
579 detailed description is provided in the text.

580

581 **Figure 4.** A portion of the detector image, for the post-heating X-ray measurement
582 shown in Figure 3, prior to integration and conversion to a one-dimensional diffraction
583 pattern. The labels are the hkl's for the magnesite reflections observed in the integrated
584 patterns.

585

586 **Figure 5.** Ratio of lattice parameters, *a* and *c*, for the magnesite formed in this study
587 compared to what has been observed by previous workers. The dashed vertical line roughly
588 indicates the pressure below which the organic solvent pressure-transmitting media of
589 previous workers would be in a liquid state and thus truly hydrostatic.
590
591 **Figure 6.** Change in molar volume (ΔV) for the magnesite-forming reaction upon
592 temperature quench. The molar volumes were determined from the unit-cell volumes
593 observed in this study using Z=4 for CO_2-I (Downs and Somayazulu 1998), CO_2-V (Datchi et
594 al. 2012) and MgO, Z=6 for magnesite, and Z=24 for CO_2-IV (Datchi et al. 2009). The solid
595 curves were determined using EoS data for magnesite (Fiquet et al. 2002), MgO (Jacobsen et
596 al. 2008), CO_2-I (Giordano et al. 2010) and CO_2-V (Datchi et al. 2012).
597
598 **Tables 1-3** Summary of all crystalline phases observed for each heating experiment with
599 the measured pressures indicated both before and after heating. Parenthetical values represent
600 uncertainty in the last digit.

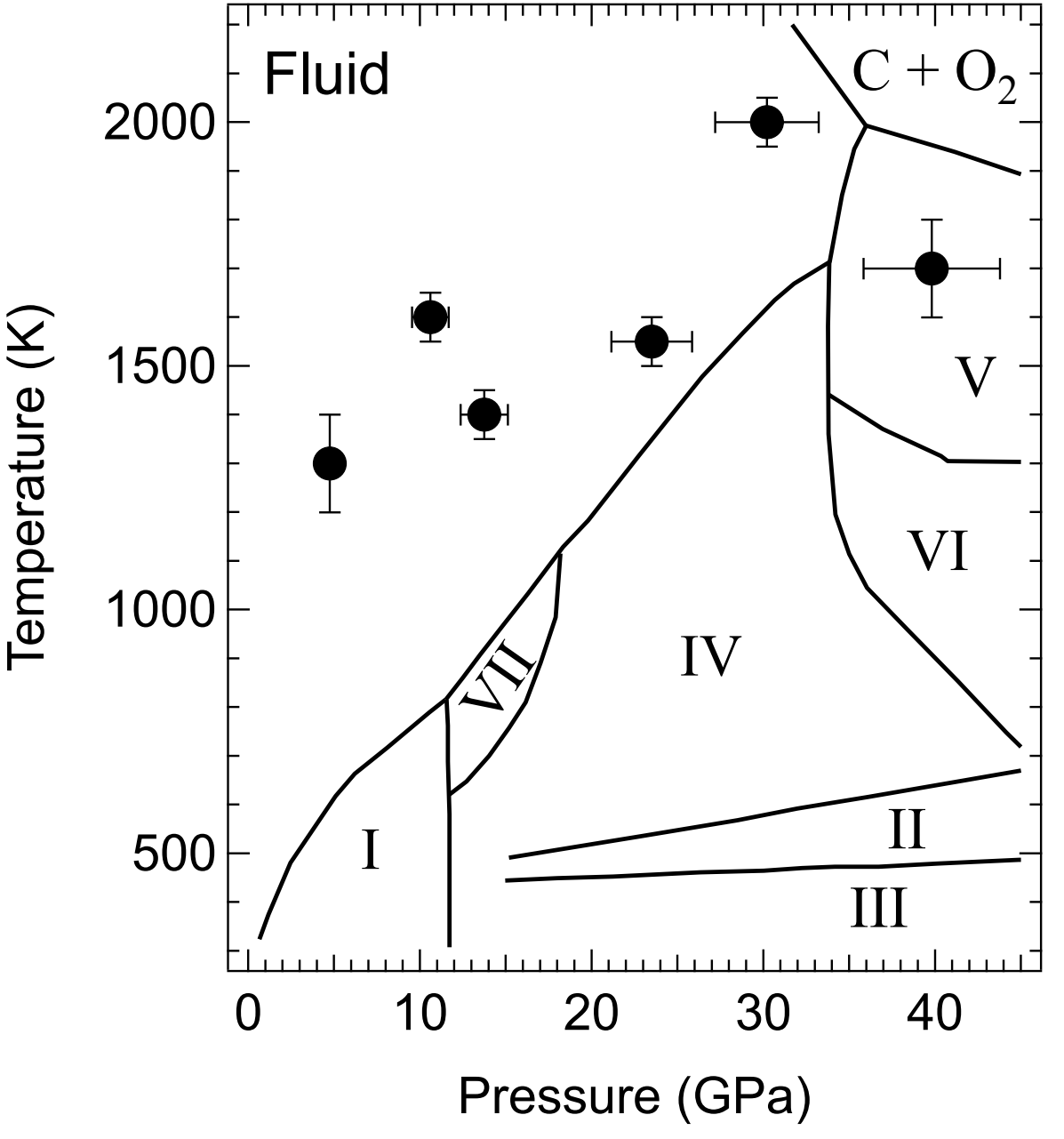
Fluid
C + O2
2000
1500
1000
500
Temperature (K)
0
10
20
30
40
Pressure (GPa)
I
II
III
IV
V
VI
VII

A

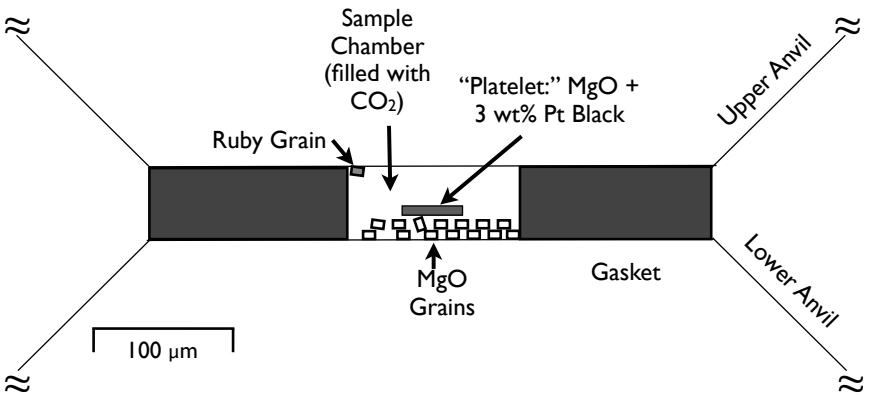
Sample
Chamber
(filled with
CO_2)
"Platelet:" MgO +
3 wt% Pt Black
Ruby Grain
Upper Anvil
Lower Anvil
MgO
Grains
Gasket
100 μm

B

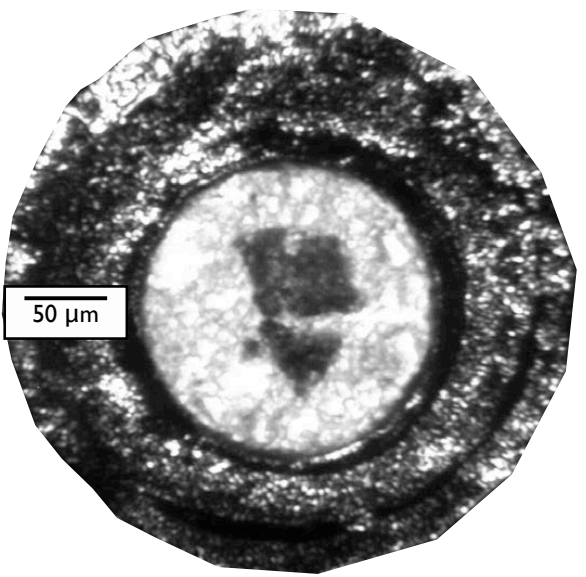
50 μm

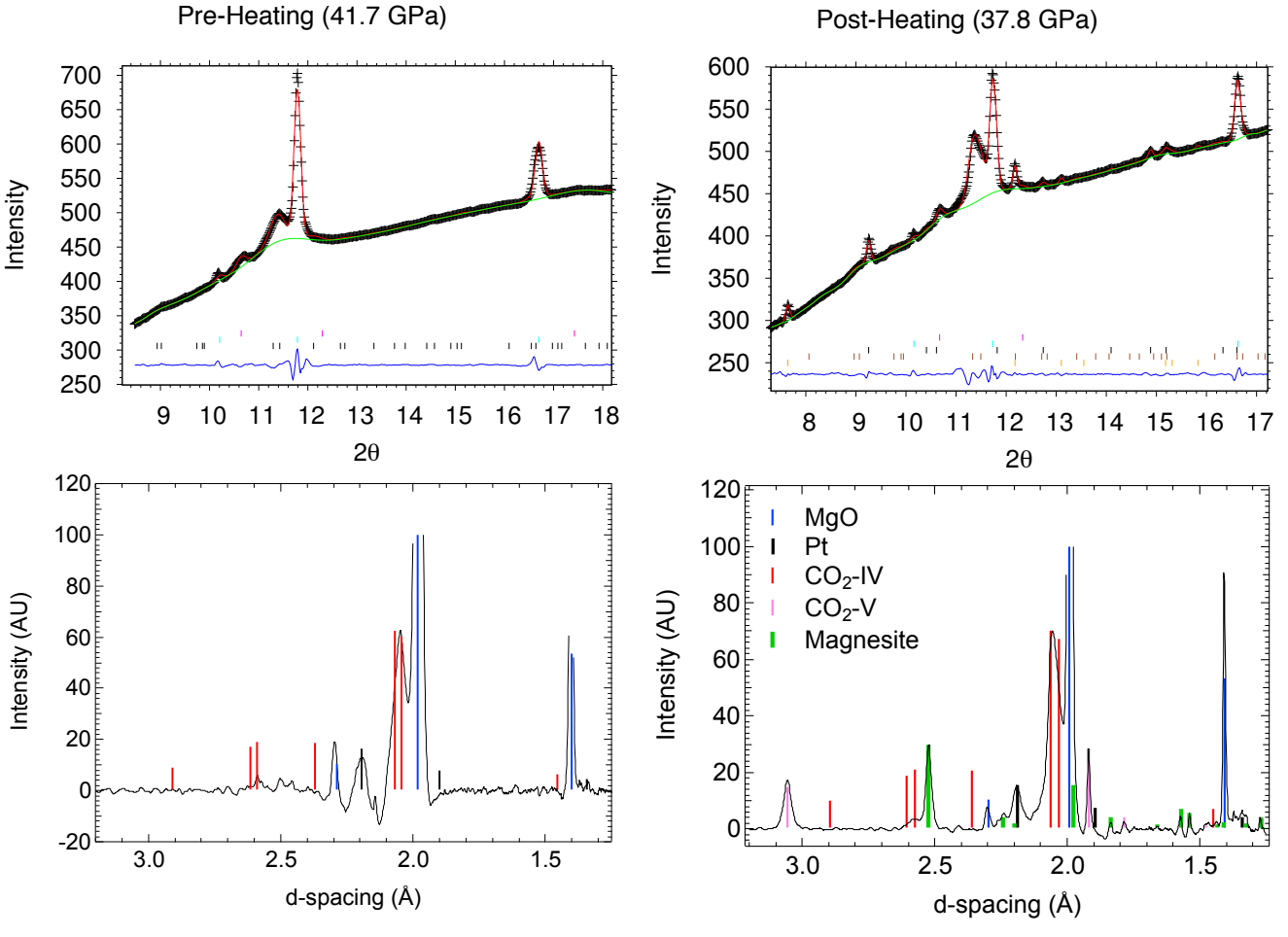
Pre-Heating (41.7 GPa)
Post-Heating (37.8 GPa)
Intensity
2θ
Intensity (AU)
d-spacing (Å)
MgO
Pt
CO2-IV
CO2-V
Magnesite

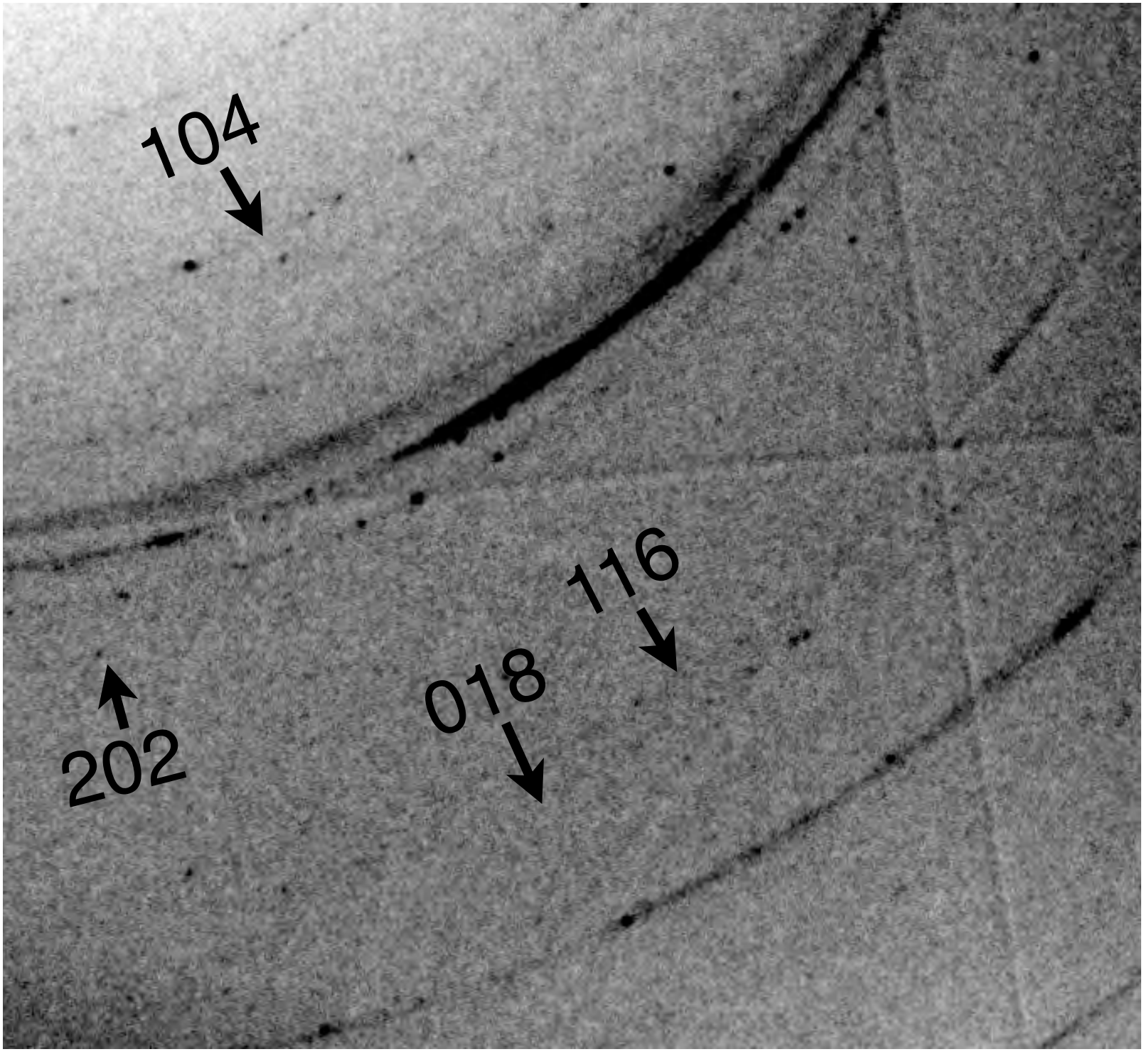
104
116
018
202

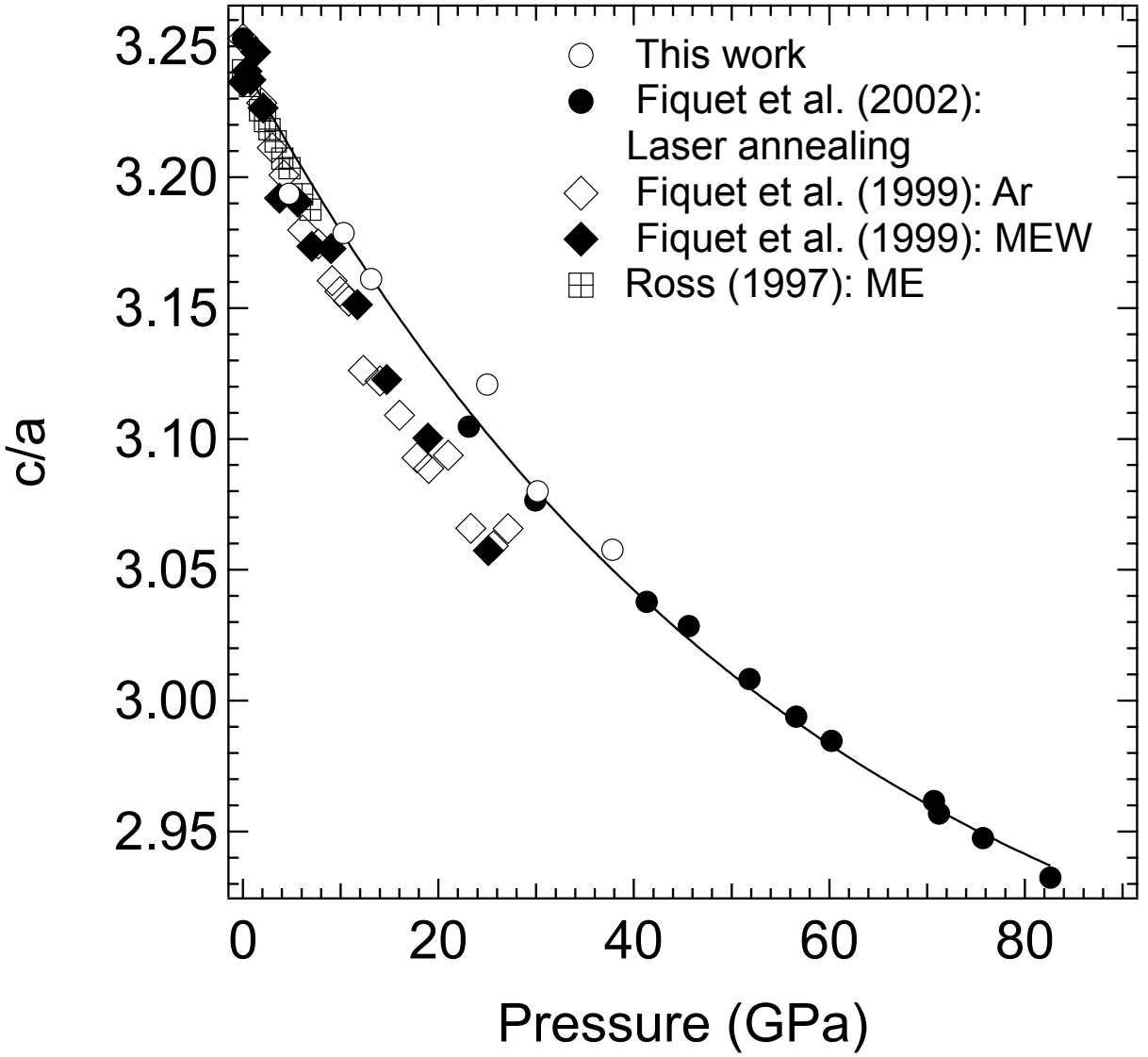
This work
Fiquet et al. (2002): Laser annealing
Fiquet et al. (1999): Ar
Fiquet et al. (1999): MEW
Ross (1997): ME
c/a
3.25
3.20
3.15
3.10
3.05
3.00
2.95
0
20
40
60
80
Pressure (GPa)

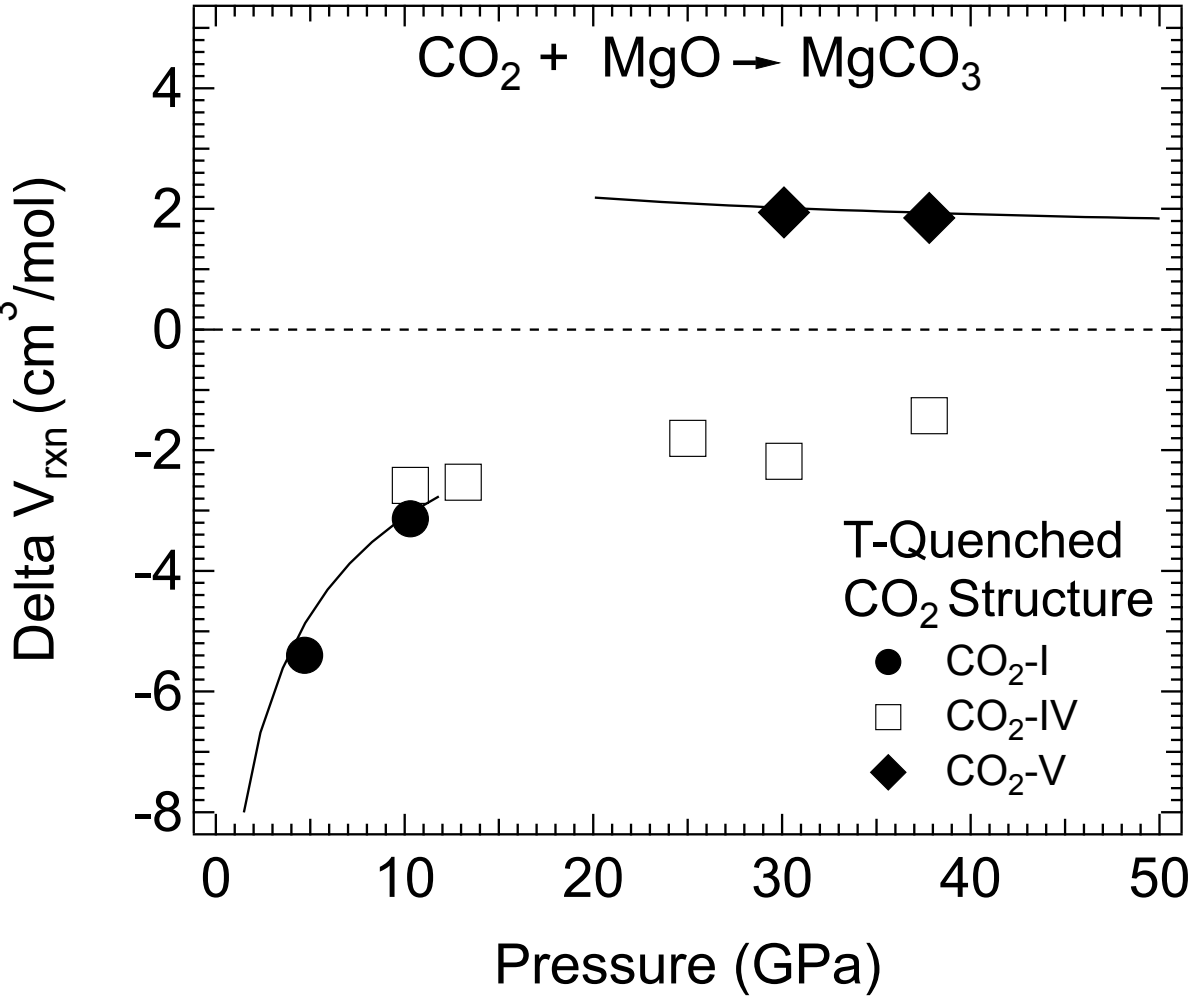
CO2 + MgO → MgCO3
Delta Vrxn (cm3/mol)
4
2
0
-2
-4
-6
-8
0
10
20
30
40
50
Pressure (GPa)
T-Quenched
CO2 Structure
CO2-I
CO2-IV
CO2-V

Table 1: CO_2 Initially as CO_2-I

P (GPa)	Phase	a (Å)	c (Å)	V (Å^3)
Pre: 4.8	**MgO**	4.1730(2)		72.67(1)
	Pt	3.904(3)		59.5(1)
	CO_2-I	5.1826(1)		139.20(1)
Post: 4.7	**MgO**	4.1734(2)		72.69(1)
	Pt	3.8989(3)		59.27(2)
	CO_2-I	5.2366(10)		143.59(8)
	Magnesite	4.6081(5)	14.717(5)	270.64(6)
Pre: 10.9	**MgO**	4,1287(1)		70.378(7)
	Pt	3.854(2)		57.24(9)
	CO_2-I	4.9426(9)		120.76(7)
Post: 10.3	**MgO**	4.1331(1)		70.602(4)
	Pt	3.8695(2)		57.94(1)
	CO_2-I	4.960(3)		122.0(3)
	CO_2-IV	8.7934(8)	10.603(4)	710.0(3)
	Magnesite	4.5403(3)	14.432(1)	257.66(2)

Table 2: CO_2 Initially as CO_2-III

P (GPa)	Phase	a (Å)	b (Å)	c (Å)	V (Å^3)
Pre: 14.4	**MgO**	4.1060(1)			69.220(5)
	Pt	3.884(1)			58.58(6)
	CO_2-III	4.393(2)	4.562(4)	5.838(3)	117.0(1)
Post: 13.1	**MgO**	4.1143(1)			69.649(5)
	Pt	3.8644(1)			57.710(5)
	CO_2-IV	8.699(1)		10.641(3)	697.3(2)
	Magnesite	4.5249(5)		14.304(1)	253.63(4)
Pre: 22.0	**MgO**	4.0609(2)			66.97(1)
	Pt	3.840(2)			56.63(1)
	CO_2-III	4.22(1)	4.55(1)	5.791(9)	111.3(1)
Post: 25.0	**MgO**	4.0446(2)			66.16(1)
	Pt	3.8493(3)			57.04(1)
	CO_2-II	3.546(1)		4.2405(8)	53.31(2)
	CO_2-IV	8.475(1)		10.479(4)	651.9(2)
	Magnesite	4.4876(4)		14.005(1)	244.25(3)

Table 3: CO_2 Initially as CO_2-IV

P (GPa)	Phase	a (Å)	c (Å)	V (Å^3)
Pre: 30.3	**MgO**	4.0170(1)		64.820(4)
	Pt	3.831(1)		56.22(6)
	CO_2-IV	8.410(3)	10.197(9)	624.5(7)
Post: 30.1	**MgO**	4.0179(1)		64.863(7)
	Pt	3.8164(6)		55.58(3)
	CO_2-IV	8.417(2)	10.210(3)	626.5(2)
	CO_2-V	3.608(1)	5.917(3)	77.03(2)
	Magnesite	4.4318(5)	13.650(2)	232.18(3)
Pre: 41.7	**MgO**	3.9643(1)		62.304(5)
	Pt	3.801(2)		54.93(6)
	CO_2-IV	8.177(3)	10.193(9)	590.3(4)
Post: 37.8	**MgO**	3.9817(2)		63.126(9)
	Pt	3.791(2)		54.49(8)
	CO_2-IV	8.130(2)	10.174(2)	582.4(2)
	CO_2-V	3.568(1)	5.913(4)	75.28(3)
	Magnesite	4.4030(9)	13.463(5)	226.08(8)